Evidence for hindrance in fusion between sulfur and lead nuclei

J. Khuyagbaatar,[1,*] K. Nishio,[2] S. Hofmann,[1] D. Ackermann,[1] M. Block,[1] S. Heinz,[1] F. P. Heßberger,[1] K. Hirose,[3] H. Ikezoe,[2] B. Kinlder,[1] B. Lommel,[1] H. Makii,[2] S. Mitsuoka,[2] I. Nishinaka,[2] T. Ohtsuki,[3] Y. Wakabayashi,[2] and S. Yan[4]

[1]*GSI Helmholtzzentrum für Schwerionenforschung, 64291 Darmstadt, Germany*

[2]*Advanced Science Research Center, Japan Atomic Energy Agency, Tokai, Ibaraki 319-195, Japan*

[3]*Laboratory of Nuclear Science, Tohoku University, Sendai, Japan*

[4]*China Institute of Atomic Energy, P.O. Box 275 (10), Beijing, China*

(Received 24 February 2012; revised manuscript received 6 October 2012; published 3 December 2012)

The influence of the structure of projectile and target nuclei on the capture cross sections was investigated for the reactions ^{34}S + ^{204,206,208}Pb and ^{36}S + ^{204,206,208}Pb. Capture cross sections were deduced by measuring the fission fragments using multiwire proportional counters. An enhancement of the capture cross sections relative to a one-dimensional barrier penetration model was observed for all reactions at energies below the interaction barriers. The enhancement is larger in the case of reactions with ^{34}S than with ^{36}S. This observation is explained by a stronger coupling to the vibrational states in the reactions with ^{34}S. Comparing the capture cross sections and the evaporation-residue cross sections for the reactions ^{36}S + ^{206}Pb and ^{34}S + ^{208}Pb, both yielding the same compound nucleus ^{242}Cf, it is shown that the latter reaction has a lower fusion probability.

DOI: 10.1103/PhysRevC.86.064602 PACS number(s): 25.70.Jj, 25.70.Gh

I. INTRODUCTION

The most successful method for the production of heavy and superheavy nuclei is the fusion of two colliding nuclei forming an excited compound nucleus (CN), which de-excites by evaporation of light particles, preferably neutrons, resulting in a cold evaporation residue (ER) [1,2]. However, excited CN can also decay into two fragments (CN fission). The probability depends on the fissility parameter, excitation energy and angular momentum of the formed CN. These so-called fusion-evaporation and fusion-fission reactions represent the complete fusion-reaction channel of the colliding nuclei.

However, the system formed by the projectile and target nuclei can also reseparate before fusion due to the strong repulsive Coulomb force in the so-called quasifission process. In general, the fragments from quasifission have significantly different mass and angular distributions than the fragments from a fusion-fission reaction.

The sum of the cross sections of complete fusion including fusion-fission and particle evaporation and quasifission represents the capture cross section. In the case of heavy CN, the cross section deduced from the sum of fragments of fusion-fission and quasifission reactions (fission cross section) represents a good approximation to the capture cross section, because the ER cross section is small.

The so-called fusion hindrance of the colliding nuclei can be determined as the ratio of quasifission and capture cross sections. Fusion hindrance depends strongly on the properties of nuclei in entrance channel of the reaction, i.e., on charge, mass and deformation of projectile and target [3]. As a result, the fusion probability for the formation of a certain CN can differ significantly using different combinations of projectile and target.

The choice of a suitable projectile-target combination as well as an optimum beam energy are crucial for a successful synthesis of the heaviest nuclei. In this respect, the study of reactions resulting in the same CN, but using different projectiles and targets, is especially interesting, because the data result in information on the reaction mechanism in the entrance channel.

One pair of such reactions is ^{36}S + ^{206}Pb and ^{34}S + ^{208}Pb, both yielding the same CN ^{242}Cf. Evaporation residue cross sections of the $2n$ channel have been measured in [4] for the first time. The values reported there were (5.0 ± 2.5) nb and (1.0 ± 1.5) nb, respectively, with the reaction ^{36}S + ^{206}Pb having a cross section about five times larger than that for ^{34}S + ^{208}Pb. This difference was attributed to the different reaction Q value which is more negative for the reaction with the semimagic nucleus ^{36}S, resulting, at the same CN excitation energy, in a higher fusion probability. However, in this experiment only the fission fragments from the produced ER's were measured and ER cross sections were deduced taking into account an estimated spontaneous fission branching of 0.02.

Recently, we have measured the ER cross sections for the $2n$ and $3n$ channels of these two reactions using an improved experimental technique allowing for detection of both α and spontaneous fission decays of the produced ER's [5,6]. The measured cross section for the $2n$ channel of ^{36}S + ^{206}Pb was approximately 25 times larger than that of ^{34}S + ^{208}Pb. In the case of the $3n$ channel an approximately ten times larger cross section was measured for ^{36}S + ^{206}Pb than for ^{34}S + ^{208}Pb. These values were obtained near the maxima of the $2n$ and $3n$ cross sections.

In this work we studied effects of the entrance channel on reactions with beams of ^{36}S and ^{34}S and targets of the lead isotopes ^{204}Pb, ^{206}Pb, and ^{208}Pb. The data are compared with coupled-channels (CC) calculations. Finally, the obtained fission cross sections for the reactions ^{36}S + ^{206}Pb and ^{34}S + ^{208}Pb were used as input data for a cross-section calculation in order to explain the difference between the ER cross sections of these two reactions.

*J.Khuyagbaatar@gsi.de

II. EXPERIMENTAL SETUP

The experiment was performed at the JAEA tandem accelerator laboratory in Tokai, Japan. Beams of ^{34}S and ^{36}S were extracted from the negative ion source and were accelerated to energies of $E_{\rm lab} = (160 - 200)$ MeV. Beam intensities were in the range from 0.1 to 3.0 pnA ($1\,p\text{nA} = 6.24 \times 10^9$ particles/s). Metallic lead targets with thicknesses of 100 μg/cm^2 were prepared at the GSI target laboratory. They were produced by evaporating metallic, isotopically enriched (>99.9%) material of ^{204}Pb, ^{206}Pb, and ^{208}Pb on carbon foils having a thickness of approximately 40 μg/cm^2. The opposite side of the targets was covered with a 10 μg/cm^2-carbon layer. The targets were mounted at an angle of 45° to the beam axis with the thin carbon layer upstream. The experimental setup and the analysis procedure were similar to that described in [7].

Two position-sensitive multiwire proportional counters (MWPCs) were used for detecting both fission fragments in coincidence. The emission angles $\theta_{\rm i}$ ($i = 1, 2$) and out-of-plane angles $\varphi_{\rm i}$ of the fission fragments are defined in Fig. 1. They were determined by the incident positions of the fragments on the MWPCs. The MWPC consists of a gold coated mylar foil (cathode), which is sandwiched by two grounded wire planes. The wire planes were made of stretched gold-coated tungsten wires with a 2 mm pitch. The active area of the MWPC is 200 mm in horizontal and 120 mm in vertical direction. The entrance windows of the MWPC were made of Mylar films of 3 μm thickness. The detectors were operated with isobutane gas at a pressure of 3 mbar.

The counters MWPC1 and MWPC2 were located at a distance of 211 mm from the target at angles $\theta_1 = -57.0°$ and $\theta_2 = +90.0°$, respectively. They covered a range of $-82.0° \leqslant \theta_1 \leqslant -32.0°$ and $65.0° \leqslant \theta_2 \leqslant 115.0°$. The covered out-of-plane angles were $72.0° \leqslant \varphi_1 \leqslant 108.0°$ at $\theta_1 = -57.0°$ and $74.1° \leqslant \varphi_2 \leqslant 105.9°$ at $\theta_2 = +90.0°$. The folding angle θ_{12} and the out-of-plane angle φ_{12} are defined as $\theta_1 + \theta_2$ and as $\varphi_1 + \varphi_2$, respectively.

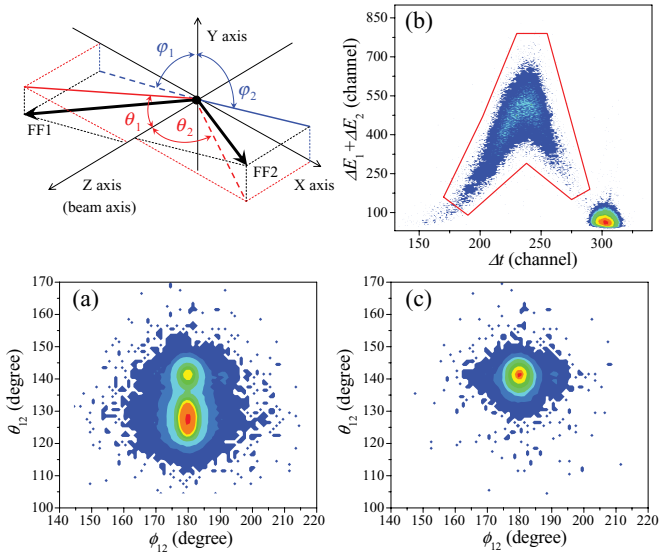

FIG. 1. (Color online) Upper left: definition of the emission angles θ_1 and θ_2 and of the out-of-plane angles φ_1 and φ_2, under which the fission fragments FF1 and FF2 are emitted. (a) Measured events plotted in the φ_{12} vs θ_{12} plane. (b) Events plotted in the Δt and $(\Delta E_1 + \Delta E_2)$ plane. (c) Same as (a), but obtained with a gate on the events marked in (b).

The time difference Δt between the signals from the cathodes of the two MWPCs was measured. The charges induced in both MWPCs contain information on the energy deposition ΔE_1 and ΔE_2 of particles traversing the active area between the cathode and the wire planes. The accumulated beam dose was deduced by detecting elastically scattered beam particles within a solid angle of 1.96 msr at an angle of +26.5° relative to the beam axis.

Examples from the analysis of fission fragments from the ^{34}S + ^{208}Pb reaction are shown in Fig. 1. The data were obtained at the center-of-mass energy $E_{\rm c.m.} = 158.7$ MeV (in the middle of the target). Figure 1(a) shows the events in a $(\varphi_{12}, \theta_{12})$ plot. Fission events are observed at $\theta_{12} = 141°$ and events from elastic scattering at $\theta_{12} = 128°$. In the $(\Delta t, \Delta E_1 + \Delta E_2)$ plot Fig. [1(b)] these events are well separated.

The polygon plot around the events shown in Fig. 1(b) marks the selected fission events. Figure 1(c) shows the fission events marked in Fig. 1(b) in the $(\varphi_{12}, \theta_{12})$ plot. The total number of these events, which could include events from quasifission as well as events from fission of the CN, were used for determining the fission cross sections.

In reactions with lead targets, lead-like nuclei produced in transfer reactions have excitation energies smaller than the fission barrier. Therefore, fission of such reaction products was not observed. This is different in reactions using actinide targets, where fission of target-like nuclei produced by nucleon-transfer reactions occurs, however, at different folding angles [7].

III. RESULTS AND DISCUSSION

The measured fission cross sections are shown in Fig. 2 as function of $E_{\rm c.m.}/V_{\rm int}$, where $V_{\rm int}$ is the height of the interaction barrier (see below). The cross sections were deduced from the fragment angular distribution $d\sigma_{\rm fiss}/d\theta_{\rm c.m.}$ in the range of $85° \leqslant \theta_{\rm c.m.} \leqslant 125°$. The function $W(\theta_{\rm c.m.})$ defined in [8] was fitted to the data of the angular distribution. The integration of this function over the scattering angle yielded the fission cross section. The errors include systematic uncertainties arising from the limited angular range covered by the detectors as well as from statistical fluctuations. The measured excitation functions are very similar within the set of data measured with one projectile, ^{36}S or ^{34}S, for all three target isotopes ^{204,206,208}Pb. However, comparing the data obtained with ^{36}S and ^{34}S, we observe higher cross sections in the sub-barrier region in the case of the reactions with ^{34}S. This indicates a larger number of open entrance channels or an increased softness in the entrance channel of the reaction.

In order to discuss the influence of nuclear structure on the capture cross section, we performed CC calculations using the code CCFULL [11]. A potential depth (Woods-Saxon) of 200 MeV [10] was chosen for all reactions. For the interaction

TABLE I. Variable $Z_1Z_2/(A_1^{1/3}+A_2^{1/3})$, reaction Q value, interaction barrier ($V_{\rm int}$) used in the present CC calculations, and barrier ($V_{\rm Bass}$) according to the Bass prediction [9] of the reactions ^{34,36}S + ^{204,206,208}Pb.

Reaction	$Z_1Z_2/(A_1^{1/3}+A_2^{1/3})$	Q value (MeV)	$V_{\rm int}$ (MeV)	$V_{\rm Bass}$ (MeV)
^{36}S + ^{208}Pb	142.19	−113.9	141.1	144.8
^{36}S + ^{206}Pb	142.49	−113.8	141.7	145.1
^{36}S + ^{204}Pb	142.78	−113.8	142.4[a]	145.4
^{34}S + ^{208}Pb	143.16	−111.0	142.7	145.7
^{34}S + ^{206}Pb	143.46	−111.7	143.2[a]	146.0
^{34}S + ^{204}Pb	143.76	−112.4	143.7	146.3

[a]Values from [10].

barriers $V_{\rm int}$, radius and diffuseness parameters were taken from [10] in the case of the reactions ^{34}S + ^{206}Pb and ^{36}S + ^{204}Pb. The values are listed in Table I ($V_{\rm int}$) and Fig. 2 (r_0 and a). The $V_{\rm int}$ values of the other reactions were estimated by linearly scaling the barrier height with $Z_1Z_2/(A_1^{1/3}+A_2^{1/3})$ from the data given in [10]. These values deviate from the barriers of the Bass model, $V_{\rm Bass}$ [9], which are also given in Table I. Radius and diffuseness parameters of these reactions were determined in the same way as the values obtained in [10] in order to reproduce the estimated interaction barriers $V_{\rm int}$. Reaction Q values, third column in Table I, were calculated using atomic mass data compiled in [12].

The results of the CC calculations are shown in Fig. 2. Dashed curves are the results without coupling (one-dimensional barrier penetration). The experimental data at energies above the interaction barrier $V_{\rm int}$ are well described by the calculation with the radius and diffuseness parameters given in the figure. However, the experimental data at sub-barrier energies are underestimated.

The cross sections are well reproduced in the reactions using ^{206}Pb and ^{208}Pb target nuclei, even at the lowest measured energies, when coupling to the first 2^+ and 3^- states of the sulfur and lead nuclei, respectively, is included. Energies and deformation parameters of these states are listed in Table II. Energy and deformation of the 3^- states in ^{204}Pb, ^{206}Pb, and ^{208}Pb vary only smoothly. Therefore, the excitation functions below the interaction barrier are similar within the set of data with the same projectile but different target isotopes. Energy and deformation of the 2^+ vibrational state in ^{36}S and ^{34}S are significantly different. The lower energy and larger deformation of the 2^+ state in ^{34}S explains the increased softness and thus increased cross sections in the sub-barrier region of reactions with ^{34}S.

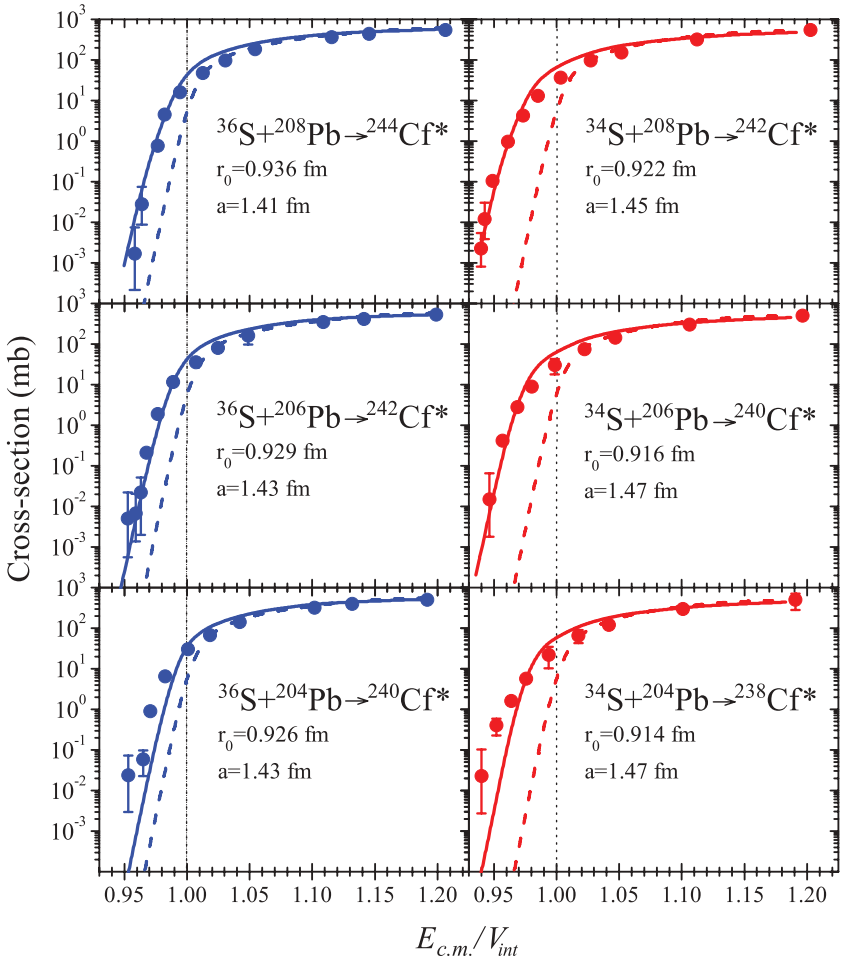

FIG. 2. (Color online) Measured fission cross sections (solid circles) plotted as a function of the ratio of center-of-mass energy and height of the interaction barrier. Solid and dashed curves represent the coupled-channels calculations (code CCFULL) with and without coupling to vibrational states, respectively. Values of the radius and diffuseness parameters r_0 and a used in the calculations are given. Vertical dotted lines indicate the position of the interaction barrier $V_{\rm int}$.

TABLE II. Spin and parity (λ^{π}), energy (E^*), and deformation parameter (β_λ) of low-lying states of the nuclei used in the reactions studied here. The values were taken from [13,14] for use in the CCFULL code of the coupled-channels calculation.

Nuclei	λ	E^* (MeV)	β_λ
^{36}S	2^+	3.291	0.164
^{34}S	2^+	2.127	0.252
^{208}Pb	3^-	2.615	0.150
^{206}Pb	3^-	2.648	0.108
^{204}Pb	3^-	2.618	0.092

In the case of ^{204}Pb, the measured cross sections are apparently larger than the calculated ones for both reactions with ^{36}S and ^{34}S projectiles. This deviation of the data from the calculation cannot be explained by the coupling to transfer channels, because the Q values for one-neutron pick-up channels are negative for all of the reactions and for reactions with ^{204}Pb even more negative than in the other two cases. A reason for the higher cross section could be the coupling to additional vibrational states in ^{204}Pb or an increased softness in the entrance channel.

Two of the reactions, ^{36}S + ^{204}Pb and ^{34}S + ^{206}Pb, result in the same CN ^{240}Cf, another two, ^{36}S + ^{206}Pb and ^{34}S + ^{208}Pb, in the same CN ^{242}Cf. For these latter reactions, ER cross sections for $2n$ and $3n$ channels were measured in previous experiments [5,6]. Comparing these data with the capture cross sections (quasifission plus CN fission) measured here, opened a possibility to obtain information on differences in the fusion probability of the two reactions.

We assumed that the capture cross section is the sum of the quasifission cross section, the fusion-fission cross section, and the ER cross section. Because the total fission cross section could not be decomposed into quasifission and CN fission cross sections, we calculated the ER cross sections with the statistical code HIVAP [15], normalizing the HIVAP capture cross section to the measured capture cross sections. The survival probability that the excited CN evaporates neutrons in competition with fission is a function of the excitation energy and angular momentum of the CN, which is calculated and taken into account in the HIVAP code. Thus, a comparison between the experimental ER cross sections and those calculated with HIVAP results in information on fusion.

In the HIVAP code we modified the parameters for the survival probability of ^{242}Cf* such that the measured ER cross sections of the ^{36}S + ^{206}Pb were reproduced at $E^* = 25.5$ and 33.1 MeV for the $2n$ and $3n$ channels, respectively (see Fig. 3).

The ER cross sections of the ^{34}S + ^{208}Pb reaction producing the same CN ^{242}Cf* were calculated, consequently, using the same survival probability as before for ^{36}S + ^{206}Pb. In addition, the parameters of the calculations of the capture cross sections were fitted to describe the measured capture cross sections (see Fig. 3).

Experimental and calculated cross sections of $2n$ and $3n$ evaporation channels of the ^{36}S + ^{206}Pb and ^{34}S + ^{208}Pb reactions are given in Table III. The ratio between the experimental and calculated ER cross sections, ($\sigma_{exp}/\sigma_{cal}$),

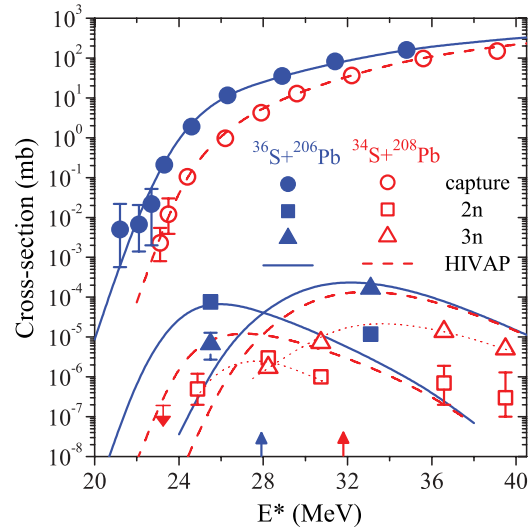

FIG. 3. (Color online) Comparison of capture and ER cross sections as function of the excitation energy of the reactions ^{36}S + ^{206}Pb (filled symbols, solid lines) and ^{34}S + ^{208}Pb (open symbols, dashed lines), both forming the same compound nucleus ^{242}Cf. The downward arrow marks an upper cross-section limit, upward arrows mark the positions of the interaction barriers. Solid and dashed lines represent the results HIVAP calculations [15] for the ER cross sections using as input for the capture cross sections the results of the coupled-channels calculation. Whereas the ER cross sections of the reaction ^{36}S + ^{206}Pb are well reproduced, the data of the reaction ^{34}S + ^{208}Pb (connected by the dotted line to guide the eye) are overestimated.

is used to reveal the discrepancies between the ER cross sections relative to the capture cross sections of these two reactions. Statistically more significant values are obtained by the geometric mean value of $\sigma_{exp}/\sigma_{cal}$ of the data

TABLE III. Experimental and calculated (HIVAP) ER cross sections of the reactions ^{36}S + ^{206}Pb [5] and ^{34}S + ^{208}Pb [6] (see also Fig. 3).

Reaction	E^* (MeV)	Evap chan	σ_{exp} (nb)	σ_{cal} (nb)	$\sigma_{exp}/\sigma_{cal}$
^{36}S + ^{206}Pb	25.5	$2n$	76 ± 10	65	1.2
		$3n$	7^{+6}_{-4}	1.0	7.0
	33.1	$2n$	12^{+5}_{-4}	3.0	4.0
		$3n$	165 ± 20	220	0.75
^{34}S + ^{208}Pb	24.9	$2n$	$0.5^{+0.7}_{-0.3}$	5.3	0.09
	28.2	$2n$	$3.0^{+0.8}_{-0.5}$	10	0.30
		$3n$	$1.7^{+1.2}_{-0.5}$	16	0.11
	30.7	$2n$	$1.0^{+0.5}_{-0.3}$	5.0	0.20
		$3n$	7^{+4}_{-2}	88	0.08
	36.6	$2n$	$0.7^{+1.2}_{-0.5}$	0.2	3.5
		$3n$	14^{+3}_{-2}	66	0.21
	39.5	$2n$	$0.3^{+1.0}_{-0.2}$	<0.1	>3
		$3n$	5^{+2}_{-1}	18	0.28

measured for the $2n$ and $3n$ channels at different excitation energies.

On the average, HIVAP underestimates the experimental ER cross sections by a factor 2.2 for the $^{36}S + ^{206}Pb$ reaction. The mean value of 2.2 was deduced as geometric mean of $\sigma_{exp}/\sigma_{cal} = 1.2, 7.0, 4.0$, and 0.75 (see Table III). Simultaneously, HIVAP overestimates the ER cross sections of the $^{34}S + ^{208}Pb$ reaction by a factor of 4.2 (see Fig. 3). This factor is deduced as the inverse of the geometric mean of 0.24 of $\sigma_{exp}/\sigma_{cal} = 0.09, 0.3, 0.11, 0.2, 0.08, 3.5, 0.21$, and 0.28 (see Table III).

Finally, a factor 9.2 (2.2/0.24) is attributed to the ratio of the ER cross sections of the reactions $^{36}S + ^{206}Pb$ and $^{34}S + ^{208}Pb$ obtained with HIVAP relative to the experimental data. Presumably, this discrepancy has to be attributed to an increase of fusion hindrance of the reaction $^{34}S + ^{208}Pb$ compared to $^{36}S + ^{206}Pb$.

In heavy ion reactions, fusion hindrance is evident for systems having Z_pZ_t values larger than 1800 [16–19]. The existence of fusion hindrance for very asymmetric reactions having Z_pZ_t values as low as 1036 and 711 was measured in an experimental study of the reactions $^{30}Si + ^{180}W$ and $^{19}F + ^{197}Au$, respectively [20]. The effect was observed in comparison to the reaction $^{12}C + ^{204}Pb$ having $Z_pZ_t = 492$. All three reactions form the same CN ^{216}Ra.

In our study the Z_pZ_t value is 1312 and the same for all reactions. The observed fusion hindrance of the reaction $^{34}S + ^{208}Pb$ relative to $^{36}S + ^{206}Pb$ cannot be attributed to different values of Z_pZ_t. However, it is experimentally evident that a difference of only two neutrons in projectile and target nuclei has such a strong influence on the fusion probability. This phenomenon cannot be explained by any model available for fusion reactions. On the experimental side the observed fusion hindrance has to be consolidated by a more complete measurement of $2n$ and $3n$ excitation functions using smaller energy steps. On a longer range the study could be extended to similar reaction pairs which differ by only two neutrons. Keeping lead isotopes as target, ideal pairs of projectiles can be found in the region of elements from oxygen to iron.

IV. CONCLUSIONS

Fission cross sections of ^{34}S and ^{36}S induced reactions with $^{204,206,208}Pb$ target nuclei were measured. The excitation functions change smoothly for the different lead isotopes. A larger enhancement of the fission cross sections in the energy region below the interaction barriers was observed in ^{34}S induced reactions compared to ^{36}S. Coupled-channels calculations which take into account the coupling to low lying vibrational states in projectile and target nuclei describe the experimental results well except for the reactions with ^{204}Pb, where the experimental fission cross sections have larger values than the calculated ones. A reason could be a coupling of more vibrational states or an increased softness in the entrance channel.

Combining data of fission and evaporation residue cross sections of the reactions $^{34}S + ^{208}Pb$ and $^{36}S + ^{206}Pb$, it was shown that the former reaction exhibits a significant hindrance of fusion relative to the reaction $^{36}S + ^{206}Pb$, in spite of the same Z_pZ_t value. For an explanation of this discrepancy more refined theoretical models are needed.

ACKNOWLEDGMENTS

We thank the JAEA-tandem facility staff for preparation of the sulfur beams. One of us (J.K.) is indebted to V. V. Sargsyan, G. G. Adamian, and N. V. Antonenko for fruitful discussions of our experimental results and theoretical calculations provided for the capture processes which, however, are not presented in this short paper. He also wants to thank JAEA for the foreign young scientist's grant which allowed for visiting JAEA and performing the experiment. This work was supported by a Grant-in-Aid for Scientific Research of the Japan Society for the Promotion of Science.

[1] S. Hofmann and G. Münzenberg, Rev. Mod. Phys. **72**, 733 (2000).
[2] Y. T. Oganessian, J. Phys. G: Nucl. Part. Phys. **34**, R165 (2007).
[3] K. Nishio, S. Hofmann, F. P. Heßberger, D. Ackermann, S. Antalic, Y. Aritomo, V. F. Comas, Ch. E. Düellmann, A. Gorshkov, R. Graeger, K. Hagino, S. Heinz, J. A. Heredia, K. Hirose, H. Ikezoe, J. Khuyagbaatar, B. Kindler, I. Kojouharov, B. Lommel, R. Mann, S. Mitsuoka, Y. Nagame, I. Nishinaka, T. Ohtsuki, A. G. Popeko, S. Saro, M. Schädel, A. Tüerler, Y. Watanabe, A. Yakushev, and A. V. Yeremin, Phys. Rev. C **82**, 024611 (2010).
[4] Y. A. Lazarev, I. V. Shirokovsky, V. K. Utyonkov, S. P. Tretyakova, and V. B. Kutner, Nucl. Phys. A **588**, 501 (1995).
[5] J. Khuyagbaatar, F. P. Heßberger, S. Hofmann, D. Ackermann, V. Comas, S. Heinz, J. Heredia, B. Kindler, I. Kojouharov, B. Lommel, R. Mann, K. Nishio, and A. Yakushev, Eur. Phys. J. A **46**, 59 (2010).
[6] J. Khuyagbaatar (to be published).
[7] K. Nishio, H. Ikezoe, S. Mitsuoka, I. Nishinaka, Y. Nagame, Y. Watanabe, T. Ohtsuki, K. Hirose, and S. Hofmann, Phys. Rev. C **77**, 064607 (2008).
[8] R. Vandenbosch and J. R. Huizenga, *Nuclear Fission* (Academic Press, New York and London, 1973).
[9] R. Bass, Phys. Rev. Lett. **39**, 265 (1977).
[10] D. J. Hinde, M. Dasgupta, N. Herrald, R. G. Neilson, J. O. Newton, and M. A. Lane, Phys. Rev. C **75**, 054603 (2007).
[11] K. Hagino, N. Rowley, and A. T. Kruppa, Comput. Phys. Commun. **123**, 143 (1999).
[12] G. Audi, A. H. Wapstra, and C. Thibault, Nucl. Phys. A **729**, 337 (2003).
[13] S. Raman, C. H. Malarkey, W. T. Milner, C. W. Nestor, and P. H. Stelson, At. Data Nucl. Data Tables **36**, 1 (1987).
[14] R. H. Spear, At. Data Nucl. Data Tables **42**, 55 (1989).
[15] W. Reisdorf, Z. Phys. A **300**, 227 (1981).
[16] J. G. Keller, K.-H. Schmidt, F. P. Heßberger, G. Münzenberg, W. Reisdorf, H.-G. Clerc, and C.-C. Sahm, Nucl. Phys. A **452**, 173 (1986).

[17] C.-C. Sahm, H.-G. Clerc, K.-H. Schmidt, W. Reisdorf, P. Armbruster, F. P. Heßberger, J. G. Keller, G. Münzenberg, and D. Vermeulen, Z. Phys. A **319**, 113 (1984).

[18] C.-C. Sahm, H.-G. Clerc, K.-H. Schmidt, W. Reisdorf, P. Armbruster, F. P. Heßberger, J. G. Keller, G. Münzenberg, and D. Vermeulen, Nucl. Phys. A **441**, 316 (1985).

[19] A. B. Quint, W. Reisdorf, K.-H. Schmidt, P. Armbruster, F. P. Heßberger, S. Hofmann, J. Keller, G. Münzenberg, H. Stelzer, H.-G. Clerc, W. Morawek, and C.-C. Sahm, Z. Phys. A **346**, 119 (1993).

[20] A. C. Berriman, D. J. Hinde, M. Dasgupta, C. R. Morton, R. D. Butt, and J. O. Newton, Nature **413**, 144 (2001).